CrossMark

ORIGINAL PAPER

Synthesis of poly(amidoamine)-graft-poly(methyl acrylate) magnetic nanocomposite for removal of lead contaminant from aqueous media

A. Pourjavadi[1] · A. Abedin-Moghanaki[1] · S. H. Hosseini[1]

Abstract Poly(amidoamine)-graft-poly(methyl acrylate) magnetic nanocomposite was synthesized via radical polymerization of methyl acrylate onto modified magnetic nanoparticles followed by the functionalization of the methyl ester groups with poly(amidoamine) dendrimer. The resulting poly(amidoamine)-graft-poly(methyl acrylate) magnetic nanocomposite was then characterized by infrared spectroscopy, transmission electron microscopy, thermogravimetric analysis, scanning electron microscope and X-ray diffraction analysis. Its application as an adsorbent for the removal of Pb(II) ions was studied. The removal capability of the adsorbent was investigated in different pH values, contact time (kinetics) and initial concentration of lead. Moreover, adsorption isotherms were investigated to describe the mechanistic feature of this nanocomposite for adsorption. Accordingly, its high adsorption capacity (310 mg/g) and efficient adsorption toward lead ions in aqueous solution were shown. To further study of the chemistry behind the adsorption process, a comprehensive density functional theory-based study was performed, and a relatively strong interaction between metal ions and adsorbent was observed based on the calculated adsorption free energies.

Keywords Magnetic nanocomposite · Adsorption · Poly(amidoamine) dendrimer · Poly(methyl acrylate)

Introduction

In the recent decades, various environmental contaminants especially water pollutants have been increased due to the development of industries and factories. Heavy metals, dyes and other organic compounds such as pesticides, polycyclic aromatic hydrocarbons and organochlorines are among the most important hazardous water contaminants. Among these contaminants, heavy metals are not biodegradable and tend to accumulate in living organisms. Many heavy metal ions are known to be toxic or carcinogenic at even relatively low concentrations (Wu et al. 2010; Zhang et al. 2013a; Repo et al. 2013). Lead is especially regarded as one of the most hazardous metals for human health, which can cause basic cellular process damages. It can also damage on the central nervous system, brain, kidney, liver and reproductive system (Gurer-Orhan et al. 2004; Campbell et al. 1981).

Nowadays, numerous well-known methods such as chemical precipitation (Pang et al. 2011), membrane filtration (Song et al. 2011), ion exchange (Wdjtowicz and Stokmosa 2002), electrochemical treatment technologies (Belkacem et al. 2008) and adsorption (Jiang et al. 2015; Ghaffari et al. 2015; Tan et al. 2012; Mahmoud et al. 2013) have been extensively explored for the removal and extraction of heavy metals from

✉ A. Pourjavadi
  purjavad@sharif.edu

[1] Polymer Research Laboratory, Department of Chemistry, Sharif University of Technology, Azadi Avenue, P.O. Box 11365-9516, Tehran, Iran

⚡ Springer

water/wastewater media. Among these water treatment methods, adsorption is one of the most effective and economic routes that have been widely used for removal of heavy metals. Various adsorbents have been applied for heavy metals uptake from contaminated water, such as activated carbon (Lee et al. 2015a), multiwalled carbon nanotubes (Kosa et al. 2012), mesoporous silica (Heidari et al. 2009; Lee et al. 2015b), agricultural wastes (Minamisawa et al. 2004), biomass and polymeric materials (Reddad et al. 2002; Ge et al. 2012). However, high price, poor regeneration, unfavorable selective adsorption and separation problem have limited the application of the mentioned adsorbents (Zhang et al. 2013a). Therefore, it is an essential subject for environmental researchers and chemists to improve the adsorption capacity, selectivity, simple recovery and easy separations of the adsorbents.

The use of magnetic nano-sized materials is one of the improved methods. Magnetic nanoparticles (MNPs) have attracted much interest, due to their potential applications such as reusability, fast kinetics and reactivity for contaminant removal. In addition, MNPs facilitate separation of adsorbent from aqueous solution using an external magnetic field (Tang and Lo 2013). Nevertheless, in order to increase its adsorption capacity and stability against acidic and alkaline media, the surface of nanoparticles was modified by some organic compounds such as glycine (Zhang et al. 2013b), natural polymers, e.g., chitosan (Liu et al. 2009) and its derivatives, poly(1-vinylimidazole) (Shan et al. 2015) as well as some copolymers, e.g., acrylic acid and crotonic acid (Ge et al. 2012). However, disadvantages such as their low surface area and long contact time limited their use in practical wastewater treatment applications (Badruddozaa et al. 2013; Crini 2005).

In this work, we fabricated a magnetic nanocomposite based on cross-linked poly(methyl acrylate) (MNC) that its surface functionalized with poly(amidoamine) dendrimer (PAMAM). Functionalization with PAMAM enhances the adsorption capacity of the adsorbent (PAMAM-MNC) compared with the other adsorbent due to increasing active sites for absorbance. Moreover, the spent contact time for the Pb^{2+} removal using PAMAM-MNC adsorbent is shorter compared with previously reported adsorbents such as activated carbon, clay minerals and other magnetic adsorbent. Adsorption ability of the prepared adsorbent on Pb(II) ions was also explored using computational method.

This research was done in polymer laboratory, Department of Chemistry, Sharif University of Technology, during the years of 2013–2015.

Materials and methods

Materials

Ferric chloride ($FeCl_3.6H_2O$), ferrous chloride ($FeCl_2.4-H_2O$), lead(II) nitrate ($Pb(NO_3)_2$), ammonia (30 %), sodium hydroxide (NaOH), hydrochloric acid, tetraethyl orthosilicate (TEOS), (3-aminopropyl)trimethoxysilane (APTS) and N,N'-methylenebisacrylamide (MBA) were purchased from Merck. Analytically pure methyl acrylate (MA) and ethylenediamine (EDA) were obtained from East of China Chemical Corporation. 2,2-Azobisisobutyronitrile (AIBN) was purchased from Daejung Chemical and Metal Company in Korea. All solvents were analytical grade, and distilled water was used.

Preparation of magnetic nanocomposite

Initially, the silica-coated Fe_3O_4 magnetic nanoparticles (MNPs) were prepared according to the previously reported procedure (Lu et al. 2007). The MNPs were then modified with APTS to establish amine groups. Typically, 2 g MNP was suspended in 60 mL toluene by ultrasonication bath. Four milliliters APTS was then added and the mixture was refluxed under stirring for 20 h. The modified MNP–NH_2 was magnetically collected and washed three times with ethanol as well as dried at 40 °C.

To prepare magnetic nanocomposite, 0.5 g MNP–NH_2 was dispersed in 20 mL dry chloroform. Five grams methyl acrylate and 0.35 g MBA were added to the above mixture. After 10 min, 0.09 g AIBN was added to the solution to initiate the polymerization reaction and the gelation process completed within 2 h. The obtained magnetic nanocomposite (MNC) was magnetically separated and washed three times with methanol.

Finally, in order to establish active sites on the MNC for the adsorption of metal ions, the surface of MNC was modified with PAMAM dendrimer. Grafting of PAMAM dendrimer onto the surface of nanocomposite was performed via method proposed by Tomalia (Bourque et al. 1999; Pourjavadi et al. 2012). EDA and MA were used to functionalize the MNC according to the following procedure. Two grams MNC was milled and dispersed in methanol.

Int. J. Environ. Sci. Technol. (2016) 13:2437–2448

2439

Excess amount of EDA (6 mL) was added to the mixture, and the mixture was refluxed under continuous stirring for 3 days. The obtained product (MNC-G1) was magnetically separated and washed with methanol. The resulted MNC-G1 was dispersed again in methanol, and excess amount of MA (6 mL) was added to flask and the mixture refluxed for 2 days. Then, the product (MNC-G1′) washed with methanol and dried at 50 °C. The last two steps were repeated twice for the formation of the next generations of PAMAM dendrimer (MNC-G2′, MNC-G3′ and PAMAM-MNC). Final product (PAMAM-MNC) was magnetically separated, washed thoroughly with methanol and dried at 50 °C.

Characterization

Thermogravimetric analysis (TGA) of samples was recorded under a nitrogen atmosphere by a TGA Q 50 thermogravimetric analyzer. Infrared (IR) spectra of all samples were obtained from KBr pellets and using an ABB Bommem MB-100 spectrometer. A TOPCON-002B electron microscope was used for taking transmission electron microscopy (TEM) images. The morphology of products was studied by scanning electron microscope (SEM) Philips, XL30. Rigalcu D/Max-3c X-ray diffractometer was used for acquiring XRD pattern. CHN analyses were performed with LECO TRUSPEC elemental analyzer. Varian AA-220 Atomic absorbent spectrophotometer was applied for determination of the concentration of metal ions in aqueous solution.

Adsorption and desorption experiments

Pb^{2+} ions adsorption experiments were performed in aqueous solution. The effect of pH, contact time, initial concentration and adsorbent amount on adsorption behavior was investigated according to the following procedures. Examining each parameter except adsorbent amount was carried out by adding 10 ± 1 mg adsorbent into 10 mL Pb^{2+} aqueous solution at room temperature and constant rate 300 rpm. The other effective parameters were kept constant during the evaluation of each parameter. At the end of each step, the adsorbents were separated by external magnetic field and residual concentrations of Pb^{2+} in solution specified using atomic absorption spectroscopy.

The metal adsorption capacity is calculated by Eq. (1):

$$Q = \frac{(C_0 - C_e)V}{m} \tag{1}$$

where Q (mg/g) is adsorption capacity, V (L) is the volume of the Pb^{2+} solution, m (g) is the adsorbent amount and C_0

(mg/L) and C_e (mg/L) are the initial and equilibrium concentration of Pb^{2+} in solution, respectively.

In order to study the reusability of PAMAM-MNC adsorbent, 0.3 g Pb(II)-loaded adsorbent was stirred into 100 mL of 0.1 M HCl for 10 min which is an optimal regenerating media for desorption of magnetic core adsorbent (Zhang et al. 2013a). Then, the adsorbent was magnetically separated and washed with methanol and water to remove unabsorbed Pb^{2+} and excess HCl. The recycled adsorbent was reused for next adsorption runs. This process was repeated five times.

Computational section

The adsorption free energies of Pb^{2+} and Cd^{2+} with a segment of PAMAM were calculated by Spartan 06 (Spartan '06V102'). The geometry optimization was performed by B3LYP/6-311++G(d,p) basis set for H, C, N and O atoms and LANL2DZ basis set for Pb^{2+} and Cd^{2+} ions. All minima were confirmed by the presence of only real vibrational frequencies, and the adsorption free energies were calculated by the following Eq. (2):

$$\Delta G_{ad...M^{2+}} = G_{ad...M^{2+}} - G_{ad} - G_{M^{2+}} \tag{2}$$

See supporting information for a summary of the optimized geometry of structures.

Results and discussion

Preparation and characterization of the adsorbent

At the beginning of this study, it was found that the synthesis of PAMAM-MNC proceeded via three steps: (1) formation of iron oxide nanoparticles via co-precipitation method, then coating of the generated iron oxide with APTS; (2) the synthesis of MNC magnetic nanocomposite; (3) modification of MNC with PAMAM dendrimer.

In the first step, the simultaneous presence of Fe^{2+} and Fe^{3+} ions in solution of ammonia leads to formation of Fe_3O_4 nanoparticles precipitate, as reported earlier (Tang et al. 2009). The generated Fe_3O_4 nanoparticles were then coated by silica, following by enrichment of their surface with amine functionality using APTS coating agent.

In the next step, MNC was prepared by cross-linking copolymerization of MA and MBA in the presence of $MNP–NH_2$. Notably, during the polymerization, magnetic nanoparticles were entrapped within the polymer matrix. Polymer chains were covalently bonded to magnetic nanoparticles by amidation of ester groups.

Scheme 1 Synthetic route of magnetic nanocomposite (MNC) and propagation of PAMAM dendrimer onto the surface of MNC
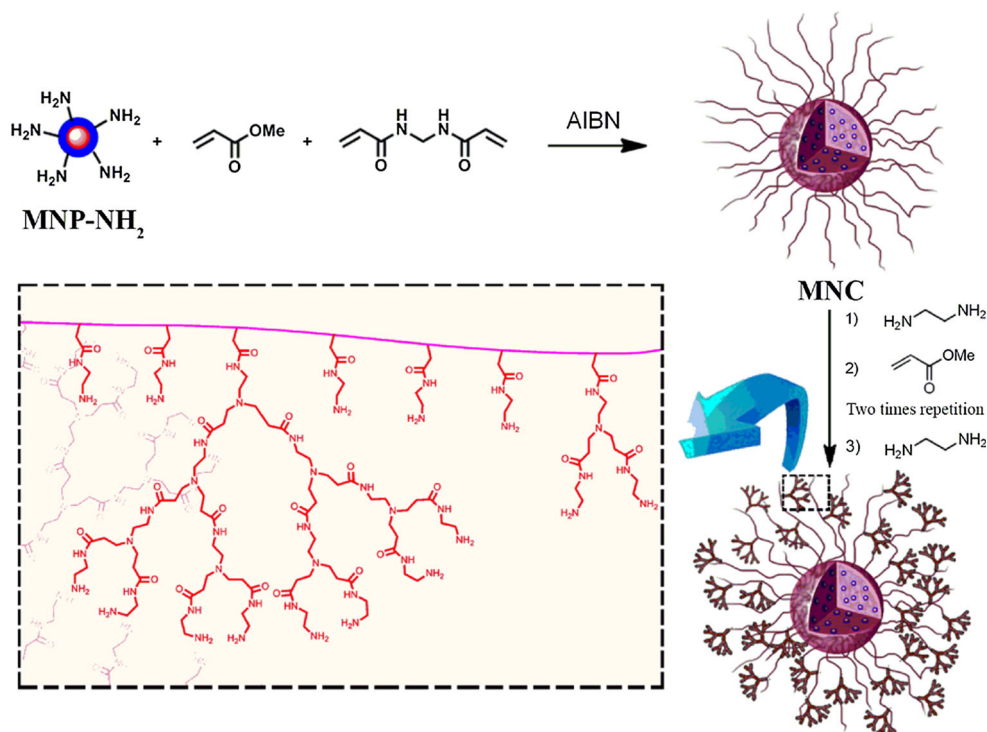

Table 1 Results of CHN analysis

Compound	C (%)	H (%)	N (%)
MNP–NH$_2$	7.041	1.042	0.738
MNC	34.660	6.040	11.890
PAMAM-MNC	47.810	7.936	20.280

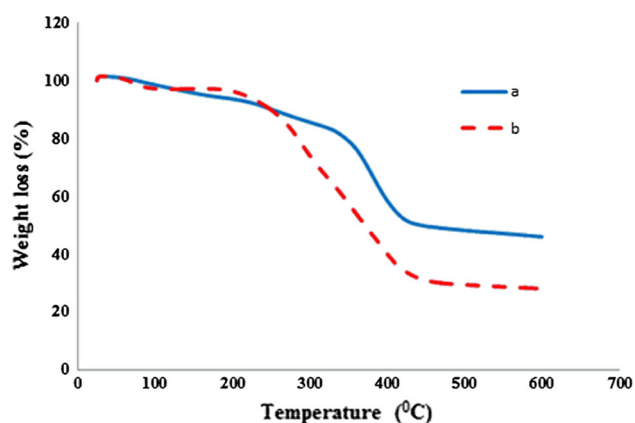**Fig. 2** IR spectra of MNP–NH$_2$ (**a**), MNC (**b**) and PAMAM-MNC (**c**)

Fig. 1 TGA curves of MNC (**a**) and PAMAM-MNC (**b**)

In the final step, propagation of PAMAM dendrimer up to the third generation was carried out via the methods pioneered by Tomalia (Bourque et al. 1999;
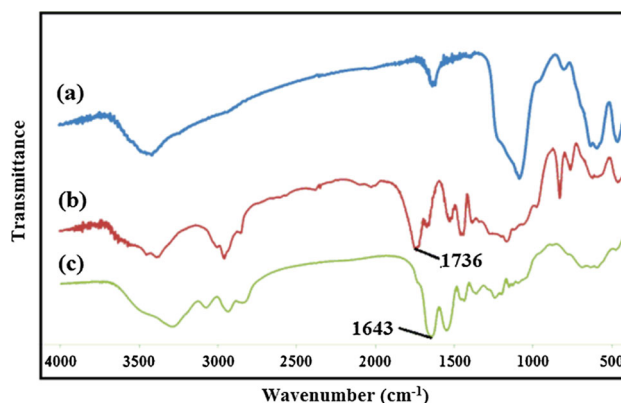
Pourjavadi et al. 2012). Accordingly, the ester groups of MNC react with the excess amount of EDA. Then, to form amino propionate ester on the MNC (MNC-G1′), a Michael-type addition was performed between –NH$_2$ groups on the surface of nanocomposite and methyl acrylate. In order to complete the first generation, subsequent amidation reaction was performed with ester groups on the surface of MNC-G1′ with EDA. Importantly, the second and third generations of the PAMAM dendrimer on the surface of nanocomposite are formed via application of the last two reactions. The synthesis of

MNC and its modification with PAMAM dendrimer are shown in Scheme 1.

The results of CHN analysis for MNP–NH$_2$, MNC and PAMAM-MNC are reported in Table 1. It is clear that, in each step of synthesis of nanocomposite, the percentage of carbon and nitrogen increased. These results in turn confirm that the MNC was successfully modified by PAMAM.

Figure 1 displays the TGA curves of MNC and PAMAM-MNC. In both TGA curves, the weight losses below 150 °C related to loss of the physically adsorbed water molecules. The weight loss from 150 to 600 °C was attributed to the thermal degradation of organic content of sample. The larger weight loss of the PAMAM-MNC compared with MNC is due to the thermal decomposition of grafted dendrimer on the MNC. The content of PAMAM dendrimer was obtained about 18 wt% according to the TGA curves.

In addition, to confirm the structure of products at each step of the synthesis of adsorbent, particularly in the development of PAMAM dendrimer onto the MNC nanocomposite, the FTIR analysis is performed (Fig. S1, see supporting information). The IR spectra of MNP–NH$_2$, MNC and PAMAM-MNC are shown in Fig. 2. In this regards, the spectrum of MNP–NH$_2$ indicates vibrations of Fe–O in 613 and 464 cm^{-1}. The presence of peaks at 798, 1104, 2940 and 3450 cm^{-1} is attributed to N–H wagging, Si–O–Si bonding, aliphatic C–H stretching and N–H stretching vibration, respectively (Tan et al. 2012). Moreover, the peak of Fe–O–Si bond overlaps with Fe–O bond peak in the range of 565–585 cm^{-1} (Yamaura et al. 2004). As shown in Fig. 2b, MNC formation was confirmed by the presence of peak 1736 cm^{-1} corresponding to stretching vibration of ester groups. It is important to mention that the ester group peak is disappeared after reaction with EDA (Fig. S1 MNC-G1, G2, G3 and PAMAM-MNC), and it appears again in the IR

spectrum after reaction with methyl acrylate (Fig. S1 MNC-G1′, G2′ and G3′). The IR spectra of all products are presented in Fig. S1.

The XRD pattern of PAMAM-MNC is depicted in Fig. 3. Six characteristic peaks of Fe$_3$O$_4$ (in 2θ values about 30, 36, 43, 53, 57 and 62) indexed by their indices (220, 311, 400, 422, 511 and 440) are observed in the XRD pattern of PAMAM-MNC. The broad peak at $2\theta = 20$ is attributed to amorphous silica phase in the nanocomposite structure. Herein, the XRD analysis demonstrates that the crystalline structure of Fe$_3$O$_4$ has not change during the synthetic steps of adsorbent.

The morphology of PAMAM-MNC, MNC and MNP–NH$_2$ was studied via the SEM and TEM analysis, as shown in Fig. S2 and Fig. 4. The SEM image of PAMAM-MNC shows a bulk structure of adsorbent. Moreover, it can be seen that the PAMAM-MNC has a rough surface and distribution of the Fe$_3$O$_4$ nanoparticles is nearly homogeneous. In TEM image of MNP–NH$_2$ (Fig. S2b), the dark points represent Fe$_3$O$_4$ nanoparticles which coated by a gray silica shell, and the TEM image of PAMAM-MNC displays that the dark MNP–NH$_2$ nanoparticles were distributed in nanocomposite matrix. The diameter of MNP–NH$_2$ was around 10–15 nm.

Effect of pH on adsorption capacity of Pb^{2+}

The pH of solution is one of the important factors that affect the adsorption behavior, due to its impact on the functional groups of the adsorbent as well as the solubility of the metal ions. Thus, adsorption should be performed in the optimum pH range. It has been shown that the Pb^{2+} ions begin to hydrolyze and form Pb(OH)$_2$ and Pb(OH)$^+$ precipitate at pH > 6, and the uptake of Pb^{2+} may be performed with the simultaneous precipitation of Pb(OH)$_2$ and Pb(OH)$^+$ (Zhang et al. 2013a; Naiya et al. 2009). Hence, the effect of pH on adsorption capacity of Pb^{2+} was studied in the pH range of 1–6 and known initial concentration of Pb^{2+} (600 mg/L). However, as shown in Fig. 5, it is clearly observed that the adsorption amounts of Pb^{2+} ions enhanced continuously with increasing of the initial pH of the solution from 1 to 6 and the adsorption amounts decreased at lower degree of pH, due to formation of positively charged –NH^{3+} and –NH$_2$$^+$– groups on the adsorbent. On the other hand, the tendency of coordination between metal cations and positively charged surface decreased because of a competition between Pb^{2+} and H$^+$ ions to coordinate with the adsorbent (Scheme 2). However, as pH value was increased, positive charge density of the adsorbent decreased and its adsorption capacity improved. The maximum adsorption capacity (310 mg/g) of Pb^{2+} was at pH 5–6.
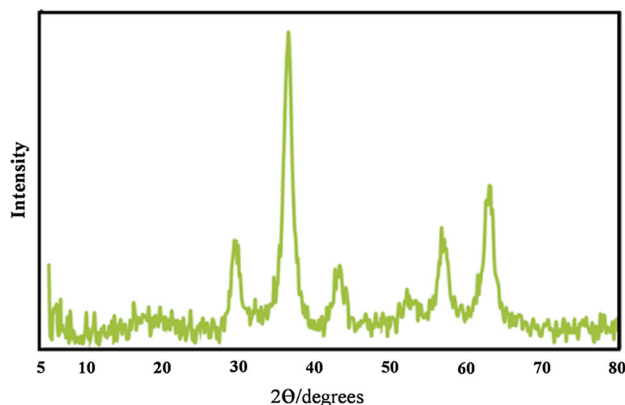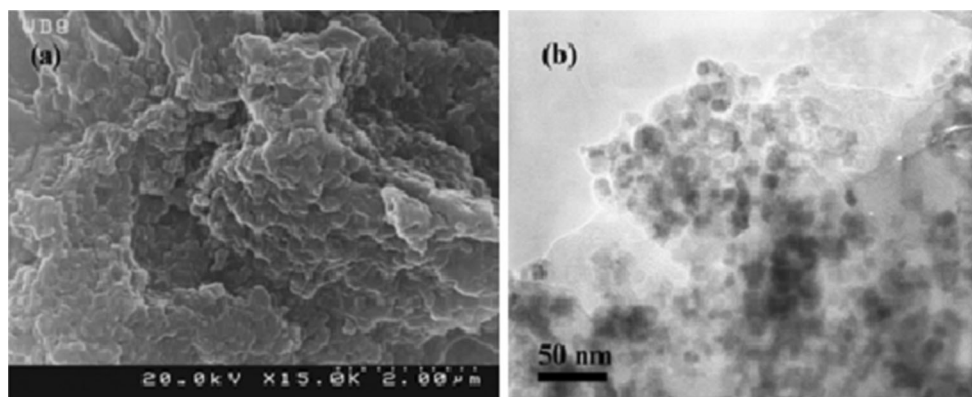

Fig. 3 XRD pattern of PAMAM-MNC

2442

Int. J. Environ. Sci. Technol. (2016) 13:2437–2448

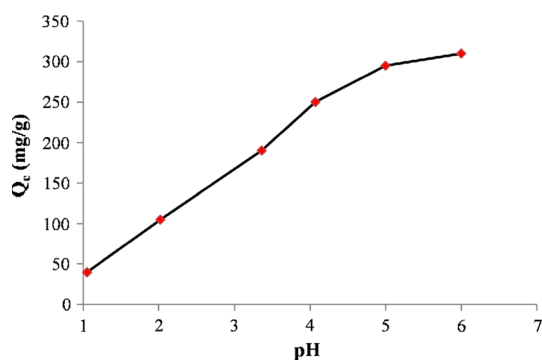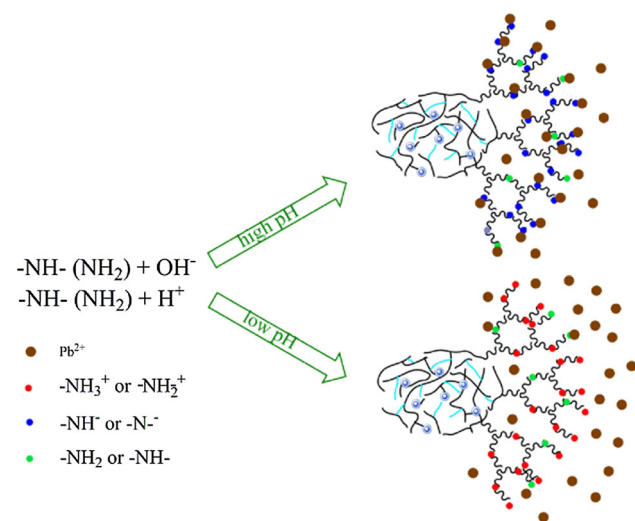**Fig. 4** SEM (**a**) and TEM (**b**) images of PAMAM-MNC

Fig. 5 Effect of solution pH on the adsorption of Pb^{2+} from aqueous solution

Scheme 2 Removal behavior of adsorbent under acidic and basic conditions
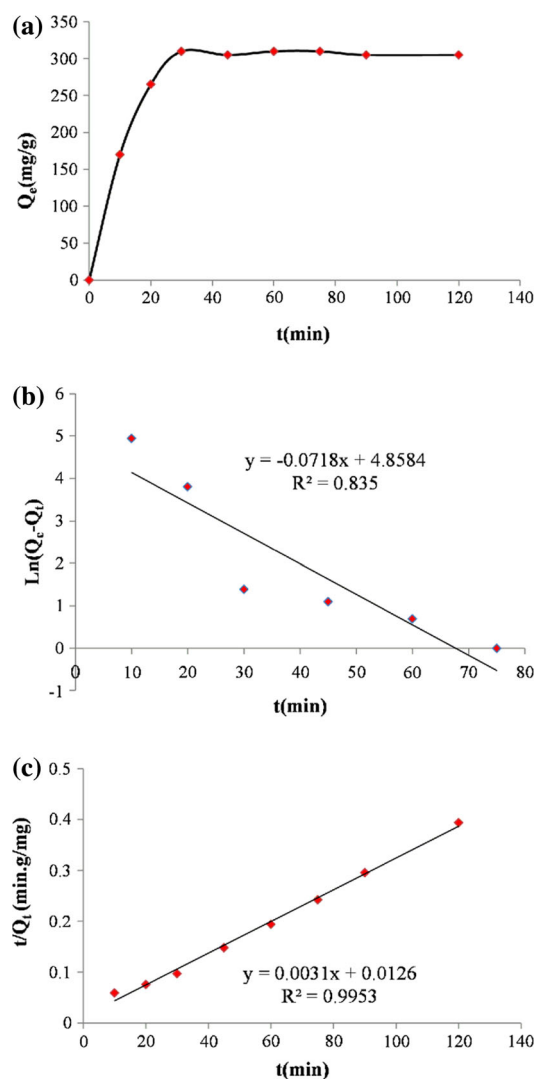

Fig. 6 Effect of contact time on the equilibrium adsorption of Pb^{2+} from aqueous solution (**a**) pseudo-first-order (**b**) and pseudo-second-order (**c**) kinetic models for Pb^{2+} removal by PAMAM-MNC

Table 2 Comparison of PAMAM-MNC with some previously reported adsorbents

Adsorbents	Q (mg/g)	pH	Time (min)	Refs.
$Fe_3O_4@SiO_2$–NH_2 core shell nanomaterials	238	5–6	480	Zhang et al. (2013a)
Amino-functionalized Fe_3O_4 MNP	40.1	5	<3	Tan et al. (2012)
Nano-Fe_3O_4–SiO_2–TETA[a]	270	7	30	Mahmoud et al. (2013)
Cyclodextrin poly-MNPs	64.5	5.5–6	45	Badruddozaa et al. (2013)
Turkish illitic clay	16.61	3	100	Shekinah et al. (2002)
Activated carbon prepared from Eichhornia	239	4	240	Ozdes et al. (2011)
Amine-functionalized mesoporous MNPs	369	5	150<	Xin et al. (2012)
KIT-6-EDTA[b]	191	5–6	<40	Ezzeddine et al. (2015)
Tetraoxalyl ethylenediamine melamine chelate resin grafted coconut active charcoal	47.7	5.5	>240	Jin et al. (2013)
Hybrid polymeric nanocomposite	49.72	7	<15	Alsohaimi et al. (2015)
PAMAM-MNC	310	5–6	30	This study

[a] Triethylenetetramine

[b] Ethylenediaminetetraacetic acid

Table 3 Kinetic parameters for pseudo-first-order and pseudo-second-order models

	$Q_{e,expt}$ (mg/g)	Pseudo-first-order kinetic model			Pseudo-second-order kinetic model			
		k_1 (min^{-1})	$Q_{e,cal}$ (mg/g)	R^2	v_0 (mg/g/min)	k_2 (g/mg/min)	$Q_{e,cal}$ (mg/g)	R^2
Pb^{2+}	310	0.0718	128.8	0.835	79.4	7.63×10^{-4}	322	0.9953

Effect of contact time and adsorption kinetics

The contact time is one of the important factors for economical wastewater treatment application (Badruddozaa et al. 2013). The adsorption of Pb^{2+} by PAMAM-MNC was studied with time ranging from 10 to 120 min. This investigation was performed in known initial concentration of Pb^{2+} (600 mg/L) and optimum pH value 5.5. The results of contact time influence on Pb^{2+} adsorption are represented in Fig. 6a. It was found that the adsorption takes place during the early stages of the removal process that may be due to the availability and abundance of active sites on the adsorbent surface. The maximum adsorption of Pb^{2+} ions was obtained almost within 30 min. During the next contact time from 30 to 120 min, the removal rate becomes quite slow through a gradual decrease in the number of active sites of the adsorbent. Interestingly, the contact time for the Pb^{2+} removal using PAMAM-MNC adsorbent is very short compared with previously reported adsorbents such as activated carbon, clay minerals and other magnetic adsorbent (see Table 2).

The adsorption kinetic of Pb^{2+} by PAMAM-MNC adsorbent was studied by means of two kinetic models: pseudo-first-order model and pseudo-second-order model according to the following equations:

$$\text{Pseudo-first-order equation:} \quad \ln(Q_e - Q_t) = \ln Q_e - k_1 t \tag{3}$$

$$\text{Pseudo-second-order equation:} \quad \frac{t}{Q_t} = \frac{1}{k_2 Q_e^2} + \frac{t}{Q_e} \tag{4}$$

where Q_t (mg/g) and Q_e (mg/g) show the adsorption capacity at time t and equilibrium state, respectively, t is the time (min) and k_1 and k_2 are the kinetic rate constants (g/mg min) of the pseudo-first-order and pseudo-second-order model (Lagergren 1898; Ho and McKay 1998).

The early adsorption rate (v_0) of Pb^{2+} was also obtained using pseudo-second-order model according to Eq. (5):

$$v_0 = k_2 Q_e^2 \tag{5}$$

Figure 6b, c shows the linear plots of Ln ($Q_e - Q_t$) versus t and t/Q_t versus t, respectively. The calculated kinetic parameters for both models are listed in Table 3. Comparison of the correlation coefficients (R^2) derived from both models was revealed that the experimental data are more consistent with the pseudo-second-order model than the pseudo-first-order model. Moreover, the experimental Q_e value is more consistent with the calculated Q_e value from the pseudo-second-order rate equation than those from pseudo-first-order rate equation.
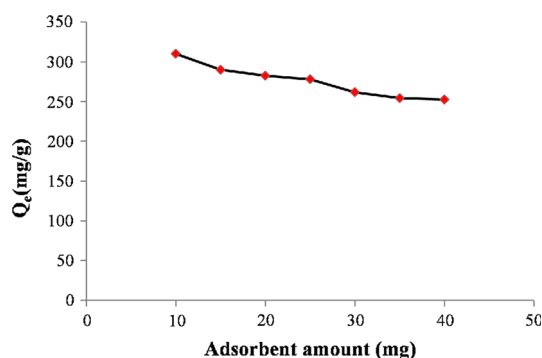
2444

Int. J. Environ. Sci. Technol. (2016) 13:2437–2448

Fig. 7 Effect of adsorbent amount on the equilibrium adsorption of Pb^{2+}
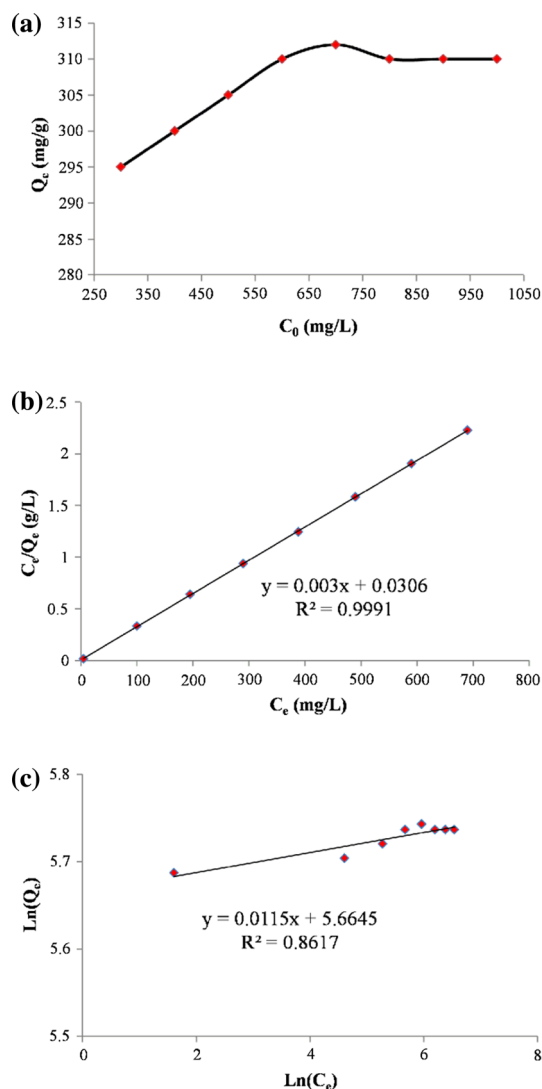

Fig. 8 Effect of Pb^{2+} initial concentration on the equilibrium adsorption of Pb^{2+} from aqueous solution (**a**) Langmuir (**b**) and Freundlich (**c**) isotherm models for Pb^{2+} removal by PAMAM-MNC

The pseudo-second-order kinetic model was developed based on the assumption that the rate-limiting steps are chemisorptions due to valence forces through electrons exchange or sharing between adsorbent and adsorbate (Heidari et al. 2009; Reddad et al. 2002). Following this model, it indicates that interaction between Pb^{2+} and PAMAM-MNC adsorbent is mainly chemical adsorption.

Effect of adsorbent dosage on adsorption capacity of Pb^{2+}

Another important parameter is the effect of adsorbent dosage on the Pb^{2+} adsorption capacity value which was studied in 10–40 mg of PAMAM-MNC, under constant conditions. Results reported in Fig. 7 showed that the removal of lead ions from solution increased by increasing adsorbent dose. However, the adsorption capacity was slowly decreased as amount of adsorbent increased. This observation is attributed to the splitting effect of flux or concentration gradient between Pb^{2+} ions and adsorbent (Metin et al. 2013).

Effect of initial Pb^{2+} concentration and adsorption isotherms

The effect of the initial Pb^{2+} concentration (ranging from 300 to 1000 mg/L) onto the adsorption capacity of PAMAM-MNC was studied under optimum pH as shown in Fig. 8. The adsorption capacity of Pb^{2+} increases with increasing initial Pb^{2+} concentration until 600 mg/L, and then it remains constant.

In addition, to study the adsorption isotherm, two isotherm models introduced by Langmuir and Freundlich were applied (Foo and Hameed 2010). The Langmuir model is represented according to Eq. (6):

$$\frac{C_e}{Q_e} = \frac{C_e}{Q_m} + \frac{1}{Q_m k_l} \tag{6}$$

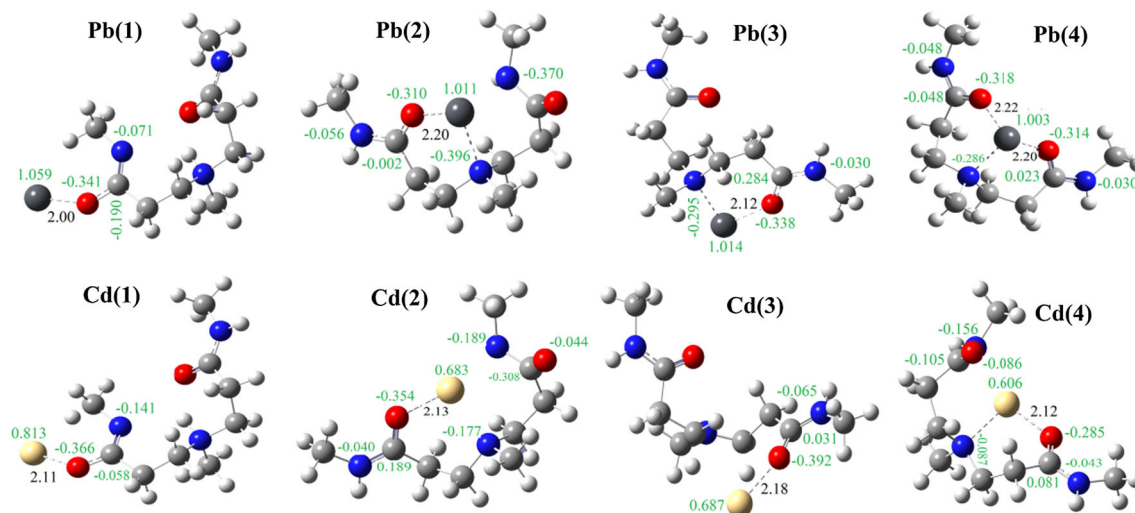while Freundlich isotherm equation can be represented as Eq. (7):

$$\ln Q_e = \ln k_F + \frac{1}{n} \ln C_e \tag{7}$$

where Q_e and Q_m (mg/g) show the equilibrium and maximum adsorption capacity of Pb^{2+}, C_e (mg/L) is the equilibrium Pb^{2+} concentration and k_l and k_F are the Langmuir and Freundlich adsorption constants,

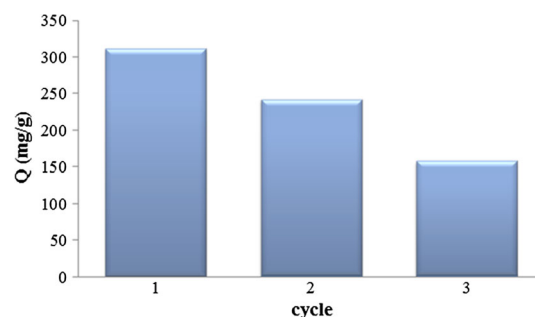**Table 4** Adsorption isotherm parameters of Langmuir and Freundlich models

	Langmuir isotherm model				Freundlich isotherm model		
	Q_{max} (mg/g)	k_1 (L/mg)	R^2	R_1	k_F (mg$^{1-(1/n)}$ L$^{1/n}$/g)	n	R^2
Pb^{2+}	333	0.098	0.999	0.0101–0.0329	288.4437	86.96	0.8617

Fig. 9 Optimized models of Pb^{2+} and Cd^{2+} ions interaction with different sites of a segment of PAMAM dendrimer

Table 5 Adsorption free energies (kcal/mol) between lead and cadmium ions with different sites of a segment of PAMAM dendrimer as calculated at the B3LYP method

	ΔG (kcal/mol)			
	1	2	3	4
Pb(II)	167.2	181.0	177.5	211.7
Cd(II)	173.1	207.4	176.6	210.5

Fig. 10 Reusability of the adsorbents

respectively. The plots of C_e/Q_e versus C_e and $\ln(Q_e)$ versus $\ln(C_e)$ were obtained in a linear form according to Fig. 8b, c. Table 4 lists the calculated constants and correlation coefficients of Langmuir and Freundlich isotherms. Comparison of the correlation coefficients (R^2) derived from both models indicated that Langmuir model provides a better fit of the experimental data and properly describes adsorption behavior of Pb^{2+} on the prepared adsorbent.

Moreover, Langmuir model can be applied to predict the type of adsorption process using dimensionless equilibrium factor R_1 (Zhang et al. 2013a):

$$R_1 = \frac{1}{1 + k_1 C_0} \tag{8}$$

where C_0 (mg/L) is the initial concentration of Pb^{2+}. R_1 value indicates the adsorption process could be favorable as $0 < R_1 < 1$ or unfavorable as $R_1 > 1$. When R_1 is 0 or 1, the type of adsorption process is irreversible or linear, respectively. Accordingly, in this study, the R_1 value given in Table 4 indicates favorable adsorption between lead ions and the prepared adsorbent.

2446

Int. J. Environ. Sci. Technol. (2016) 13:2437–2448

Computational study

Computational methods such as density functional theory (DFT) are valuable tools for understanding the chemical reactivity systems (Zhao et al. 2014). Therefore, in order to analyze metal adsorption onto the PAMAM-MNC and to further elucidate the adsorption mechanism, theoretical calculations were performed applying density functional theory (DFT) method (Saleh et al. 2013). The adsorption free energies of Pb(II) and Cd(II) toward various positions of a segment of PAMAM-MNC were calculated, as shown in Fig. 9, and the results are summarized in Table 5. The predicted adsorption free energies of Pb(II) and Cd(II) are in the range of (167–212 kcal/mol) and (173–210 kcal/mol), respectively. The adsorption free energies between both metal ions and all sites revealed strong interaction between metal ions and adsorbent. Nevertheless, the lead and cadmium ions interaction with adsorbent in Pb4 and Cd4 situations is stronger compared with the other studied situations (see Fig. 9). Moreover, the point charges and bond length r (Pb–O and Cd–O) were also calculated and results are indicated in Fig. 9; the less positive point charges in the Pb and Cd ions at Pb4 and Cd4 situations are in agreement with adsorption free energy results. These strong interactions between Pb(II) and PAMAM-MNC adsorbent resulted in high adsorption capacity of adsorbent, which is consistent with experimental observations.

Recovery study

For practical implementation, an efficient adsorbent should exhibit not only high adsorption capacity but also high reusability in order to reduce the overall cost of the adsorption process (Ge et al. 2012). The reusability for PAMAM-MNC adsorbent was then evaluated by comparing adsorption capacity of lead ions on regenerated and fresh adsorbent as shown in Fig. 10. It is found that although adsorption capacity of Pb^{2+} decreased after three cycles, the Q value still reaches 155 mg/L. Nevertheless, the value of Q_m is still larger than previously reported adsorbent. Therefore, our reusability studies suggest that PAMAM-MNC adsorbent can be repeatedly used as an efficient adsorbent for removal of Pb^{2+} ions from aqueous solution.

Conclusion

In conclusion, we have successfully designed and synthesized a new magnetic nanocomposite followed by modification of its surface with poly(amidoamine) dendrimer.

Then, we applied it to the uptake of Pb(II) ions from aqueous solution. IR, XRD, TGA, SEM, TEM and CHN analyses were used for characterization of the adsorbent. The effect of different experimental conditions such as solution pH, contact time, adsorbent amount and initial concentration was thoroughly investigated and optimized for obtaining an improved adsorption process. The maximum adsorption capacity for lead ion was found 310 mg/g at pH = 5–6. Notably also, kinetic study clarified that experimental data fit well with the pseudo-second-order model as opposed to pseudo-first-order model. As well, the Pb^{2+} ions adsorption is well described by Langmuir isotherm model. Moreover, theoretical calculations (DFT) predicted the high adsorption free energies of Pb(II) and Cd(II) ions toward various adsorption sites. Taken the above observations into considerations, one can conclude that PAMAM-graft-poly(methyl acrylate) can be successfully applied for removal of heavy metal, especially lead from wastewater.

References

Alsohaimi IH, Wabaidur SM, Kumar M, Khan MA, Alothman ZA, Abdalla MA (2015) Synthesis, characterization of PMDA/TMSPEDA hybrid nano-composite and its applications as an adsorbent for the removal of bivalent heavy metals ions. Chem Eng J 270:9–21

Badruddozaa AZM, Shawon ZBZ, Danie TWJ, Hidajata K, Uddin MS (2013) Fe$_3$O$_4$/cyclodextrin polymer nanocomposites for selective heavy metals removal from industrial wastewater. Carbohydr Polym 91:322–332

Belkacem M, Khodir M, Abdelkrim S (2008) Treatment characteristics of textile wastewater and removal of heavy metals using the electroflotation technique. Desalination 228:245–254

Bourque SC, Maltais F, Xiao WJ, Tardif O, Alper H, Arya P, Manzer LE (1999) Hydroformylation reactions with rhodium-complexed dendrimers on silica. J Am Chem Soc 121:3035–3038

Campbell BC, Elliott HL, Meredith PA (1981) Lead-exposure and renal-failure: does renal insufficiency influence lead kinetics. Toxicol Lett 9:121–124

Crini G (2005) Recent developments in polysaccharide-based materials used as adsorbents in wastewater treatment. Prog Polym Sci 30:38–70

Ezzeddine Z, Batonneau-Gener I, Pouilloux Y, Hamad H, Saad Z, Kazpard V (2015) Divalent heavy metals adsorption onto different types of EDTA-modified mesoporous materials: effectiveness and complexation rate. Microporous Mesoporous Mater 212:125–136

Foo KY, Hameed BH (2010) Insights into the modeling of adsorption isotherm systems. Chem Eng J 156:2–10

Ge F, Li MM, Ye H, Zhao BX (2012) Effective removal of heavy metal ions Cd^{2+}, Zn^{2+}, Pb^{2+}, Cu^{2+} from aqueous solution by

polymer-modified magnetic nanoparticles. J Hazard Mater 211–212:366–372

Ghaffari A, Husain SW, Tehrani MS, Anbia M, Azar PA (2015) Highly efficient adsorption of hexavalent chromium from the aqueous system using nanoporous carbon modified with tetraethylenepentamine. Int J Environ Sci Technol 12:1835–1844

Gurer-Orhan H, Sabir HU, Ozgunes H (2004) Correlation between clinical indicators of lead poisoning and oxidative stress parameters in controls and lead-exposed workers. Toxicology 195:147–154

Heidari A, Younesi H, Mehraban Z (2009) Removal of Ni(II), Cd(II), and Pb(II) from ternary aqueous solution by amino functionalized mesoporous and nanomesoporous silica. Chem Eng J 153:70–79

Ho YS, McKay G (1998) A comparison of chemisorption kinetic models applied to pollutant removal on various sorbents. Process Saf Environ Prot 4:332–340

Jiang R, Tian J, Zheng H, Qi J, Sun S, Li X (2015) A novel magnetic adsorbent based on waste litchi peels for removing Pb(II) from aqueous solution. J Environ Manag 155:24–30

Jin GP, Zhu XH, Li CY, Fu Y, Guan JX, Wu XP (2013) Tetraoxalyl ethylenediamine melamine resin functionalized coconut active charcoal for adsorptive removal of Ni(II), Pb(II) and Cd(II) from their aqueous solution. J Environ Chem Eng 1:736–745

Kosa SA, Al-Zhrani G, Abdel Salam M (2012) Removal of heavy metals from aqueous solutions by multi-walled carbon nanotubes modified with 8-hydroxyquinoline. Chem Eng J 181–182:159–168

Lagergren S (1898) About the theory of so-called adsorption of soluble substances. K Sven Vetenskapsakad Handl 24:1–39

Lee ME, Park JH, Chung JW, Lee CY, Kang S (2015a) Removal of Pb and Cu ions from aqueous solution by Mn_3O_4-coated activated carbon. J Ind Eng Chem 21:470–475

Lee JY, Chen CH, Cheng S, Li HY (2015b) Adsorption of Pb(II) and Cu(II) metal ions on functionalized large-pore mesoporous silica. Int J Environ Sci Technol. doi:10.1007/s13762-015-0841-y

Liu X, Hu Q, Fang Z, Zhang X, Zhang B (2009) Magnetic chitosan nanocomposites: a useful recyclable tool for heavy metal ion removal. Langmuir 25:3–8

Lu AH, Salabas EL, Angew FS (2007) Magnetic nanoparticles: synthesis, protection, functionalization, and application. Chem Int Ed 46:1222–1244

Mahmoud ME, Abdelwahab MS, Fathallah EM (2013) Design of novel nano-sorbents based on nano-magnetic iron oxide–bound-nano-silicon oxide–immobilized-triethylenetetramine for implementation in water treatment of heavy metals. Chem Eng J 223:318–327

Metin A, Çiftçi H, Alver E (2013) Efficient removal of acidic dye using low-cost biocomposite beads. Ind Eng Chem Res 52:10569–10581

Minamisawa M, Minamisawa H, Yoshida S, Takai N (2004) Adsorption behavior of heavy metals on biomaterials. J Agric Food Chem 52:5606–5611

Naiya TK, Bhattacharya AK, Das SK (2009) Adsorption of Cd(II) and Pb(II) from aqueous solutions on activated alumina. J Colloid Interface Sci 333:14–26

Ozdes D, Duran C, Senturk HB (2011) Adsorptive removal of Cd(II) and Pb(II) ions from aqueous solutions by using Turkish illitic clay. J Environ Manag 92:3082–3090

Pang FM, Kumar P, Teng TT, Mohd Omar AK, Wasewar KL (2011) Removal of lead, zinc and iron by coagulation–flocculation. J Taiwan Inst Chem Eng 42:809–815

Pourjavadi A, Hosseini SH, Hosseini ST, Aghayeemeibody SA (2012) Magnetic nanoparticles coated by acidic functionalized poly(amidoamine) dendrimer: effective acidic organocatalyst. Catal Commun 28:86–89

Reddad Z, Gerente C, Andres Y, Cloirec PL (2002) Adsorption of several metal ions onto a low-cost biosorbent: kinetic and equilibrium studies. Environ Sci Technol 36:2067–2073

Repo E, Warchol JK, Bhatnagar A, Mudhoo A, Sillanpaa M (2013) Aminopolycarboxylic acid functionalized adsorbents for heavy metals removal from water. Water Res 47:4812–4832

Saleh TA, Gupta VK, Al-Saadi AA (2013) Adsorption of lead ions from aqueous solution using porous carbon derived from rubber tires: experimental and computational study. J Colloid Interface Sci 396:264–269

Shan C, Ma Z, Tong M, Ni J (2015) Removal of Hg(II) by poly(1-vinylimidazole)-grafted $Fe_3O_4@SiO_2$ magnetic nanoparticles. Water Res 69:252–260

Shekinah P, Kadirvelu K, Kanmani P, Senthilkumar P, Subburam V (2002) Adsorption of lead (II) from aqueous solution by activated carbon prepared from Eichhornia. J Chem Technol Biotechnol 77:458–464

Song J, Oh H, Kong H, Jang J (2011) Polyrhodanine modified anodic aluminum oxide membrane for heavy metal ions removal. J Hazard Mater 187:311–317

Spartan '06V102', Wavefunction, Inc, Irvine

Tan Y, Chen M, Hao Y (2012) High efficient removal of Pb(II) by amino-functionalized Fe_3O_4 magnetic nano-particles. Chem Eng J 191:104–111

Tang SCN, Lo IMC (2013) Magnetic nanoparticles: essential factors for sustainable environmental applications. Water Res 47:2613–2632

Tang B, Yuan L, Shi T, Yu L, Zhu Y (2009) Preparation of nano-sized magnetic particles from spent pickling liquors by ultrasonic-assisted chemical coprecipitation. J Hazard Mater 163:1173–1178

Wdjtowicz A, Stokmosa A (2002) Removal of heavy metal ions on smectite ion-exchange column. Pol J Environ Stud 11:97–101

Wu S, Li F, Xu R, Wei S, Li G (2010) Synthesis of thiol-functionalized MCM-41 mesoporous silicas and its application in Cu(II), Pb(II), Ag(I), and Cr(III) removal. J Nanopart Res 12:2111–2124

Xin X, Wei Q, Yang J, Yan L, Feng R, Chen G, Du B, Li H (2012) Highly efficient removal of heavy metal ions by amine-functionalized mesoporous Fe_3O_4 nanoparticles. Chem Eng J 184:132–140

Yamaura M, Camilo RL, Sampaio LC, Macedo MA, Nakamura M, Toma HE (2004) Preparation and characterization of (3-aminopropyl)triethoxysilane-coated magnetite nanoparticles. J Magn Magn Mater 279:210–217

Zhang J, Zhai S, Li S, Xiao Z, Song Y, An Q, Tian G (2013a) Pb(II) removal of $Fe_3O_4@SiO_2–NH_2$ core–shell nanomaterials

2448

Int. J. Environ. Sci. Technol. (2016) 13:2437–2448

prepared via a controllable sol–gel process. Chem Eng J 215–216:461–471

Zhang YR, Wang SQ, Shen SL, Zhao BX (2013b) A novel water treatment magnetic nanomaterial for removal of anionic and cationic dyes under severe condition. Chem Eng J 213:258–264

Zhao F, Tang WZ, Zhao D, Meng Y, Yin D, Sillanpää M (2014) Adsorption kinetics, isotherms and mechanisms of Cd(II), Pb(II), Co(II) and Ni(II) by a modified magnetic polyacrylamide microcomposite adsorbent. J Water Process Eng 4:47–57